BBA - Biomembranes 1868 (2026) 184528

Contents lists available at ScienceDirect

BBA - Biomembranes

journal homepage: www.elsevier.com/locate/bbamem

Research paper

Bicelles stabilize a compact conformation of opsin with enhanced α-helical packing

Patryk Kamil Bielski [a], Justyna Bożek [b], Valerio Marino [c], Daniele Dell'Orco [c], Carsten Dosche [b], Izabella Brand [b,d,*], Karl-Wilhelm Koch [a,d,*]

[a] Carl von Ossietzky Universität Oldenburg, Department of Neuroscience, 26129, Oldenburg, Germany
[b] Carl von Ossietzky Universität Oldenburg, Institute for Chemistry, 26111, Oldenburg, Germany
[c] Department of Neurosciences, Biomedicine and Movement Sciences, Section of Biological Chemistry, University of Verona, 37134, Verona, Italy
[d] Neuroscience Research Center for Neurosensory Sciences, Carl von Ossietzky Universität Oldenburg, 26111, Oldenburg, Germany

ARTICLE INFO

Keywords:
Bicelle
Rhodopsin
Thermal stability
Circular dichroism
Electron microscopy
Dynamic light scattering
Infrared spectroscopy
Fluorescence correlation spectroscopy
Surface plasmon resonance

ABSTRACT

Bicelles form a disc-like planar lipid bilayer surrounded by short-chain lipids at the peripheral rim. Therefore, they are well-suited to study purified transmembrane proteins in a more native-like environment. In this study, we investigated the physico-chemical properties of bicelles using transmission electron microscopy, dynamic light scattering, and fluorescence spectroscopy. The G protein-coupled receptor rhodopsin served as a prototypical membrane protein, which we reconstituted into bicelles having an average diameter of 11.6 ± 0.6 nm that increased to 14.9 ± 0.7 nm upon incorporation of rhodopsin. These results were confirmed by transmission electron microscopy and fluorescence spectroscopy. Comparing the molar concentration of bicelles and rhodopsin, we determined an average of 4 ± 1 bicelles per molecule of rhodopsin based on dynamic light scattering, and 6 ± 3 based on transmission electron microscopy data. Thus, only 14–25% of bicelles contained rhodopsin without evidence of aggregation. Infrared and circular dichroism spectroscopy measurements demonstrated that, in bicelles, rhodopsin forms a more packed structure compared to the detergent-solubilized condition, and exhibits enhanced α-helical packing. Moreover, the bicelle-reconstituted form exhibited increased thermal stability. When immobilized on sensor chip surfaces via concanavalin A anchoring, rhodopsin in bicelles showed at least a 10-fold lower binding efficiency to the G protein transducin than in detergent, although maintaining a 1:1 binding stoichiometry. These results indicate a monolamellar orientation of the bicelles on the sensor chip surface, exposing rhodopsin in native folding.

1. Introduction

Transmembrane proteins (TMPs) are found in almost all organisms, and they play critical roles in cell metabolism, inter- and intra-cellular communication, control of the membrane potential, ion homeostasis, maintenance of cell structure integrity, and cell adhesion. Investigation of the structure and function of membrane proteins in their natural environment is a major challenge because purification of TMPs requires removal of native lipids, bearing the risk of losing the native structure and function of the protein [1]. Rhodopsin is considered a benchmark membrane protein that operates as a prototypical G protein-coupled receptor in processing the light signal in photoreceptor outer segments into visual information [2]. The structure of this protein consists of seven transmembrane regions, connecting loops, an extracellular N-terminus, and a cytoplasm-facing C-terminus [3–5]. The solution of the crystal structure of rhodopsin revealed that helices account for approximately 60–70% of the secondary structure elements [6]. Next to α-helices, 3_{10}-helices have been identified in the transmembrane fragments of rhodopsin [3,7]. The remaining parts consist of β-sheets and unstructured loop regions [3,6]. Rhodopsin occupies an area of 2.8 × 3.9 nm within the membrane plane, while its height (along normal to the membrane plane) is 6.4 nm [3]. The amino acid composition of rhodopsin is dominated by hydrophobic residues, with phenylalanine (8.9%), valine (8.9%), alanine (8.3%), and leucine (8.0%) being the most abundant, contributing to the overall hydrophobic character of the protein [6].

Earlier work applying Fourier transform infrared difference spectroscopy to study rhodopsin in thin membrane films assigned fingerprint

* Corresponding authors at: Neuroscience Research Center for Neurosensory Sciences, Carl von Ossietzky Universität Oldenburg, 26111, Oldenburg, Germany.
E-mail addresses: izabella.brand@uni-oldenburg.de (I. Brand), karl.w.koch@uni-oldenburg.de (K.-W. Koch).

https://doi.org/10.1016/j.bbamem.2026.184528
Received 12 December 2025; Received in revised form 13 March 2026; Accepted 3 April 2026
Available online 7 April 2026

regions in the spectra to light-triggered conformational changes [8]. Rhodopsin activity is affected by the composition of the disc membrane in rod outer segments, which determines protein stability, kinetics, and function [9]. The lipid membranes of the rod's discs are densely filled with rhodopsin, with an average distance between the protein centers of 5.6 nm [10]. Previous work from the early 1970s stated that rhodopsin shows no restricted diffusion in the disc membrane [11,12], but this classical view was questioned by several more recent studies employing atomic force microscopy [13–15] and cryo-electron tomography [16], showing a paracrystalline or nanodomain arrangement of rhodopsin dimers (see review by Park [17] for a full account on this controversial topic). The supramolecular organization of rhodopsin is in line with a dynamic scaffolding mechanism of G protein activation by rhodopsin [18]. The molecular organization of rhodopsin in the membrane, its diffusion, and protein-protein interaction modes depend on the local lipid environment. The relationship between the lipid composition and rhodopsin functionality, although widely studied, is not yet fully understood [10,19–24].

A promising experimental approach to study the conformation of TMPs present in their native environment is the use of bicelles [1]. These are disc-shaped lipid assemblies consisting of a planar bilayer core formed by long-chain phospholipids, such as 1,2-dimyristoyl-sn-glycero-3-phosphocholine (DMPC), surrounded by a peripheral rim composed of detergent-like short-chain lipids, typically 1,2-diheptanoyl-sn-glycero-3-phosphocholine (DHPC) [25–28]. They are characterized by their q ratio, a molar ratio of long-chain lipids to the short-chain lipids, as well as the level of hydration (c_L, weight percent of total lipid mass to the total weight of the sample) [29,30]. Compared to micelles, bicelles have been shown to exhibit excellent properties in terms of protein stabilization due to the presence of a stable bilayer region in their structure [31–34]. Additionally, they serve as valuable precursors for constructing model lipid bilayers that mimic natural cell membranes [35–38]. Beyond rhodopsin, bicelles were used to stabilize and investigate other TMPs, which demonstrate their versatility as membrane mimetics. Park et al. [39] incorporated chemokine CXCR1 into bicelles, reporting usage of this medium for high-resolution solid-state NMR studies, enabling analyses of orientation, conformational dynamics, and ligand interactions. Brettmann et al. [40] reported reconstitution of ion channel domains in bicelles to probe gating and selectivity in a bilayer-like environment. Additionally, Vinothkumar [41] demonstrated that β-barrel proteins and intramembrane proteases, such as the GlpG rhomboid protease, benefit from bicelle crystallization approaches that preserve their native-like topology, as demonstrated by the successful determination of the GlpG structure in a lipid environment. In previous studies, McKibbin et al. [42] and Dong et al. [1] found that the membrane, native-like environment created by the core bilayer part of the bicelles significantly enhances the stability, folding, and functionality of rhodopsin in comparison to regular detergents like dodecyl-β-D-maltoside (DDM) or lauryldimethylamine oxide (LDAO). Rhodopsin retains proper folding and structural competence in bicelles, and circular dichroism measurements confirm that opsin maintains the α-helical structure [1,42]. Additionally, the thermal stability of rhodopsin in bicelles is improved, providing better protection against denaturation compared to widely used detergents [42]. These findings also show that bicelles are suitable assemblies to analyze rhodopsin and GPCRs in general by spectroscopic techniques.

In this work, the geometry and size of bicelles composed of lipids (DMPC core and DHPC rim) incorporating purified rhodopsin were elucidated using transmission electron microscopy (TEM), dynamic light scattering (DLS), and fluorescence spectroscopy (FCS). Quantitative analysis of the UV–vis spectra of rhodopsin in bicelles, combined with size measurements, yielded the average ratio of protein-free to rhodopsin-filled bicelles, a parameter critical for analytical applications. Furthermore, infrared (IR) spectroscopy and near-UV circular dichroism (CD) were employed to assess the secondary and tertiary structure of rhodopsin in bicelles, respectively, in comparison to the protein embedded in surfactant micelles. The binding properties of rhodopsin in bicelles were confirmed by surface plasmon resonance (SPR) studies showing interaction with the α-subunit of the G protein transducin (G_t).

2. Results

2.1. Biophysical and biochemical characterization of bicelles

The morphology, size, and stability of the bicelles were investigated by means of TEM, FCS, and DLS methods. Diluted lipid bicelle solutions were placed on TEM grids to image the morphology and size distribution of the bicelles obtained according to the procedure mentioned below. Disc-shaped aggregates were clearly visible on stained grids fabricated from bicelle solutions with total lipid concentrations ranging from 25 to 2.5 mM. TEM images of bicelle samples prepared from solutions at total lipid concentrations $\geq$ 2.5 mM appear to have an almost uniform morphology and size, see Fig. 1A. In contrast, bicelles deposited on the TEM grid from diluted samples (2.5 mM total lipid concentration) lost their structural stability and displayed irregular often spherical shapes with a broader size distribution, see Fig. 1B. Micrograph analysis included bicelle size determination. Length measurements gave an average bicelle length of 10.3 ± 1.4 nm ($n = 15$) and a height of the core, corresponding to the DMPC bilayer thickness, of 4.4 ± 0.5 nm (n = 15), as reported in Section S1, Table S1. The thickness of a DMPC bilayer (D_B) has been reported to range from 4.2 to 6.2 nm [43] depending on the physical state of the lipids and the hydration of the polar head group. Thus, the thickness of the bicelles determined in this study is in the range of the DMPC bilayer, confirming that our procedure yields well-structured DMPC/DHPC bicelles.

The size of the bicelles was further characterized using fluorescence anisotropy analysis and fluorescence correlation spectroscopy (Section S2, Fig. S1). Bicelle samples were fluorescently labeled with 9,10-bis (phenylethinyl)-anthracene (BPEA), a water-insoluble lipophilic dye whose fluorescence indicates a successful intercalation of the dye into the lipid chain region of the bicelles. [44] The location of the BPEA molecule in the hydrophobic region of the bicelle does not affect the quantitative analysis of the bicelle size, because it does not extend into the solution phase but is buried in the hydrophobic region of the aggregate. A reference measurement of isotropic BPEA in ethanol was used to estimate the measurement of the observation volume [44]. The measured translational diffusion time of the DMPC/DHPC bicelles (τ) obtained from FCS was 0.72 ms. Using this value, calibration of the observation volume with BPEA in ethanol [44] and applying the Stokes-Einstein equation, the hydrodynamic radius of the bicelles was calculated to be approximately 5.2 nm, corresponding to a diameter of 10.4 nm. This result agrees perfectly with the bicelles diameter of 10.3 nm determined from TEM micrographs. As BPEA resides within the bicelle lipid environment, the FCS-derived diffusion time reliably reflects the overall bicelle size, confirming the expected dimensions and indicating the structural integrity and homogeneity of the samples. Additionally, rotational diffusion times τ_{R_ψ} extracted from fluorescence anisotropy measurements were used to estimate an average diameter of 7.7 ± 0.3 nm ($n = 7$). This value is lower than the diameter of bicelles measured by FCS, because the model used for analyzing anisotropy data was originally established for spherical particles and not for flattened ellipsoids. Despite the error introduced by the simplified model, values for bicelle diameter are still similar to those of the other complementary methods. To exclude that that BPEA disrupts the structure of DMPC/DHPC bicelles, we systematically monitored the bicelle size using both fluorescence anisotropy and DLS (hydrodynamic diameter and PDI) across a concentration gradient of the dye (10 nM to 500 nM), as shown in Table S2 in paragraph S2. The anisotropy sizes remain consistent, varying from 7.2 nm to 8.0 nm. Those values correspond well to the previously reported diameter of 7.7 ± 0.3 nm at a 1.5 nM dye concentration.

After analyzing the size and homogeneity of the bicelles, purified

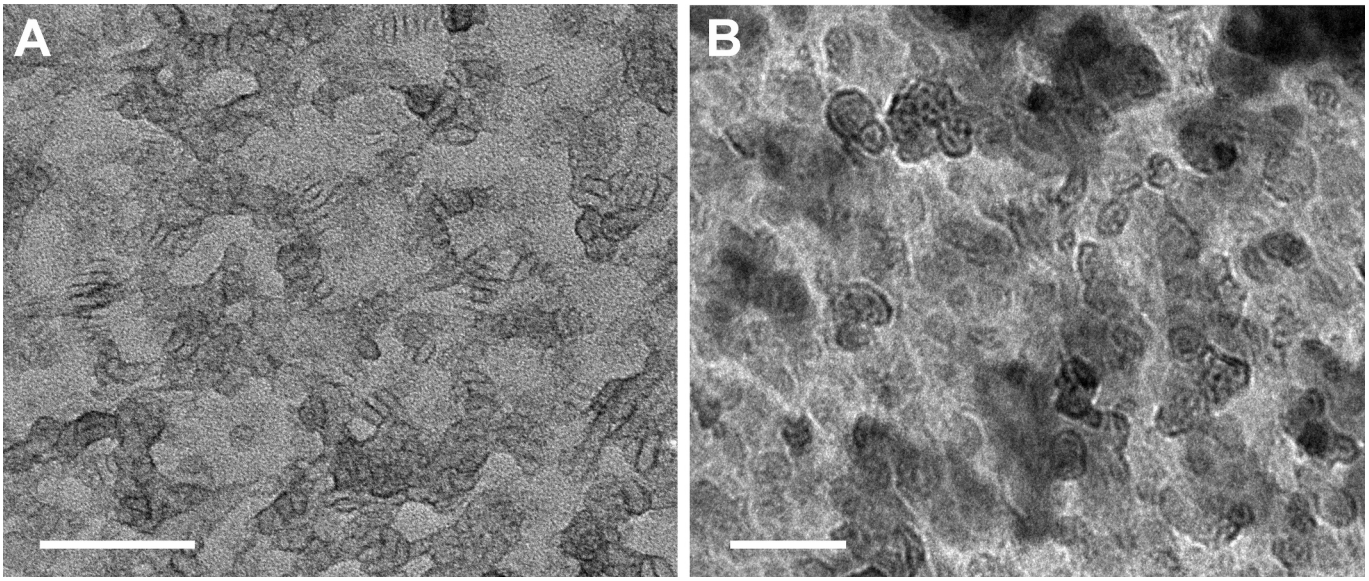

Fig. 1. TEM micrographs of bicelle samples. (A) Bicelles diluted to a final total lipid concentration of 25 mM. (B) Bicelles were diluted to a final total lipid concentration of 2.5 mM. The white scale bars in both images represent 50 nm.

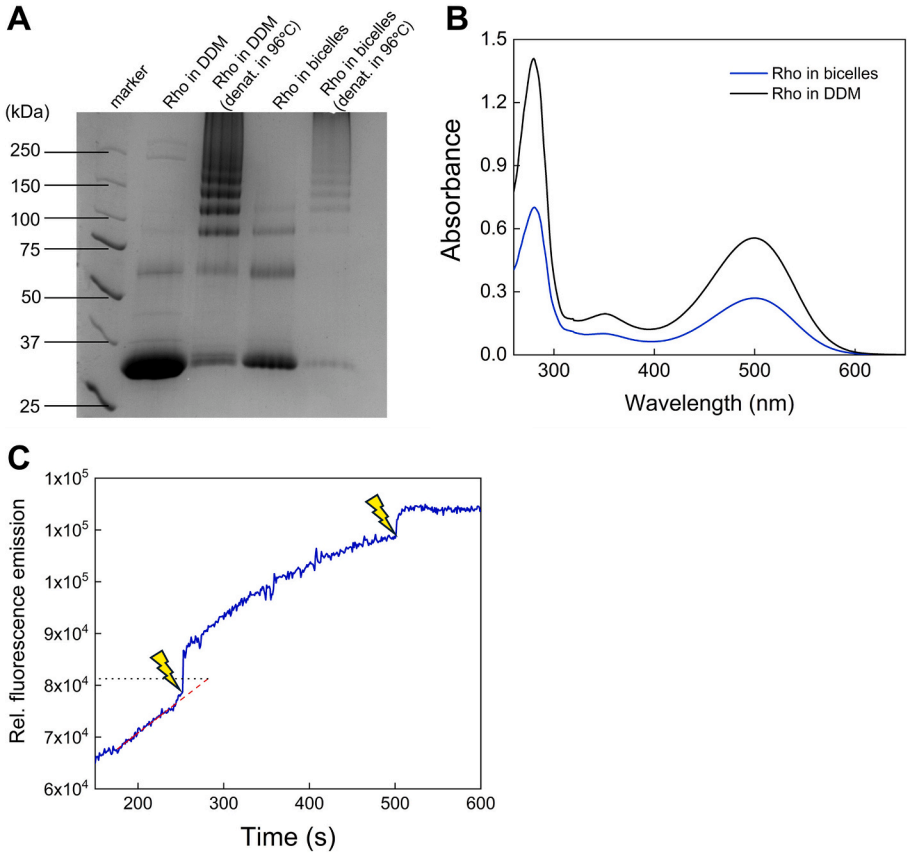

Fig. 2. Analysis of purified rhodopsin (Rho) in bicelles. (A) SDS-PAGE analysis of DDM-solubilized rhodopsin and rhodopsin in bicelles eluted from a ConA affinity column (lane 1 and 3, respectively). A 25 mM bicelles solution was applied to the column after DDM-solubilized rhodopsin was bound to ConA. Rhodopsin in bicelles was eluted with the competing carbohydrate methyl-α-mannopyranoside; Rhodopsin samples that were incubated at 96 °C for 5 min were applied in lanes 2 and 4. Heating increased the oligomer formation in both cases forming characteristic ladders. A prominent dimer of rhodopsin is visible in lanes showing rhodopsin in DDM and in bicelles, but the dimer vanished by heating the bicelles preparation thereby enforcing the building of higher oligomers. Protein bands were visualized by Coomassie Brilliant Blue staining after electrophoresis on a 10% polyacrylamide gel (raw SDS-PAGE gel in Section S3, Fig. S2). (B) UV–vis spectra of dark-adapted bovine rhodopsin reconstituted in DDM (black line) and bicelles (blue line). (C) Activation of Gt by illumination of rhodopsin in bicelles. Changes in relative fluorescence emission was recorded at 345 nm (excitation wavelength was at 300 nm), which is coupled to GDP/ GTPγS at Gt catalyzed by bleached rhodopsin. The first flash indicates illumination with white light for 30 s, the second flash was given for 5 s. The upward drift at the begin of the recording was prolonged for the time of illumination by the red line to mark the increase of fluorescence emission attributable to Gt activation, because the recording was stopped during illumination.

bovine rhodopsin was incorporated into them. To assess the fabrication of bicelles containing rhodopsin, we analyzed the purity and concentration by sodium dodecylsulfate polyacrylamide gel electrophoresis (SDS-PAGE) and UV–vis spectroscopy, respectively. SDS-PAGE analysis in Fig. 2A revealed a distinct band at ca. 35 kDa of strong intensity that was present in the rhodopsin bicelles fraction eluted from a concanavalin A (ConA) affinity column. It is consistent with the increase in the bicelle diameter to 14.9 ± 0.6 nm (n = 12), see blue dots in Fig. 3B, caused by the incorporation of rhodopsin. The intensity of this band was notably lower than that of the rhodopsin input, indicating a reduced concentration of rhodopsin in bicelles compared to rhodopsin being present in detergent DDM (left lanes in Fig. 2A). This result may indicate that the amount of bicelles was insufficient to encapsulate all rhodopsin bound to the affinity column. Additional oligomeric bands of rhodopsin between 50 and 75 kDa and above 75 kDa were observed on the gel for both preparations, rhodopsin in DDM and in bicelles. Heating the samples to 95 °C increased the formation of higher oligomers. Results are in agreement with a previous report [1].

Dynamic light scattering measurements provide insights into the size distribution and reproducibility of bicelle fabrication and their stability under varying conditions, including the presence of rhodopsin and a freezing-thawing cycle, see Fig. 3A. The average size of bicelles before and after freezing, represented by the green circles and stars in Fig. 3B, was 11.6 ± 0.6 nm (n = 12) and 11.2 ± 1.05 nm (n = 12), respectively, and agrees with TEM and FCS results. Based on the results, the bicelle stock solution can be frozen in liquid nitrogen and subsequently stored at −20 °C without significant changes in their size distribution, as shown in Fig. 3. This finding might be useful for various biomimetic, biotechnological applications.

Summarizing, the results described above confirmed the successful incorporation of rhodopsin into bicelles and indicated that the samples were compositionally homogeneous. However, the average diameter of the bicelles with rhodopsin increased to 17.2 ± 1.4 nm (n = 12) after freezing and thawing, see Fig. 3B. The post-freezing sample quality varied, with some samples containing aggregates larger than 100 nm in diameter while retaining the original pre-freezing peak, indicating condensation and clustering of the original bicelle assemblies (see lower traces in Fig. 3A); thus, the structural characterization was not performed on frozen samples.

2.2. Quantitative analysis of the bicelle size, lipid and protein concentration

We determined the ratio of the protein-free bicelles to bicelles with rhodopsin by analyzing the number of bicelles per rhodopsin as a critical parameter for characterizing our fabrication procedure. The analysis includes the determination of the molar concentration of rhodopsin in the bicelle stock solution and the geometry of the bicelle size.

The absorbance spectrum of the bicelle solution with inserted rhodopsin is shown in Fig. 2B. The distinct, intense absorption band centered at 280 nm is characteristic of tryptophan and other aromatic residues present in rhodopsin [45]. The weak band at 360 nm corresponds to *all*-trans retinal after rhodopsin bleaching [46], and the absorbance of dark-adapted rhodopsin bound to the chromophore 11-*cis*-retinal is prominent at 500 nm [47]. The average concentration of rhodopsin reconstituted in bicelles was determined from the absorbance value measured at 280 nm yielding 14.5 ± 2.8 μM (n = 5) and corresponding to the total protein content in the sample. The concentration was approximately 2.8-fold reduced relative to the initial protein concentration applied to the affinity column (40.5 ± 4.9 μM; n = 5). All values used to determine the rhodopsin concentration are provided in Section S4, Table S3. The absorbance at 500 nm, specifically for the dark-adapted, retinal-bound form of rhodopsin, indicated a concentration of 6.8 ± 1.9 μM (n = 5). The A_{280}/A_{500} ratio of 3.3 ± 0.7 (n = 5) was substantially higher than the typical value of ~1.6 observed for fully retinal-bound native rhodopsin [48].

Rhodopsin in bicelles interacted with Gt upon light activation monitored by an increase of tryptophan fluorescence (Fig. 2C). The increase in fluorescence emission at 345 nm is due to the rhodopsin catalyzed GDP/GTPγS exchange in Gt and the concomitant conformational change [48] showing that rhodopsin is functionally active.

In further analysis, the size of bicelles obtained from TEM, FCS, and DLS measurements was used to determine the number of DMPC molecules per bicelle. Details of this calculation are described in section S5a and b, Table S4, and illustrated in Fig. S3 and S4. Briefly, knowing that the rim of bicelles composed of DHPC molecules has a length of 2 nm [49], the diameter of the DMPC core of the bicelle was determined to be 6.8 ± 0.4 nm (Table S4 in Section S5a). Taking the area of the phosphatidylcholine head group (A_{HG}) of 0.6 nm^2 [50,51], the number of the DMPC molecules per core fragment of the bicelle and the concentration of bicelles were calculated (Table S4). When comparing the molar concentration of bicelles and rhodopsin ($c_{M,Rho}$ and $c_{M,DMPC}$, respectively), we determined an average of 4 ± 1 bicelles per molecule of rhodopsin based on DLS data, and 6 ± 3 based on TEM data. These results indicated an excess of free bicelles in the system, with approximately 14–25% of bicelles containing rhodopsin.

2.3. Determination of the rhodopsin structure

CD and IR spectroscopies were used to determine the secondary

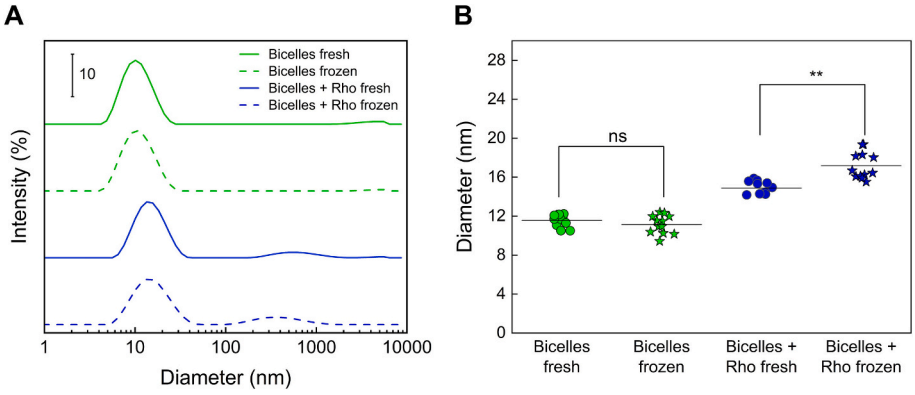

Fig. 3. Dynamic light scattering measurements. (A) DLS measurements of fresh bicelles (green line), bicelles flash-frozen in the liquid nitrogen and thawed (green dashes), fresh bicelles with inserted rhodopsin (blue line), and bicelles with inserted rhodopsin (Rho) flash-frozen in the liquid nitrogen and thawed (blue dashes). (B) Size distribution statistics from 12 biological replicates. Statistical significance was determined using a one-tailed t-test. Green dots represent fresh bicelles; green stars, bicelles flash-frozen in the liquid nitrogen (p = 0.339); blue dots, fresh bicelles with inserted Rho; and blue stars, bicelles with inserted Rho flash-frozen in the liquid nitrogen (**p = 0.002).

structure of bleached rhodopsin (opsin) embedded into bicelles. Average CD spectra in far UV (200–250 nm) were analyzed to investigate the secondary structure of opsin in bicelles (Fig. 4A, separate measurements in Section S6, Fig. S5A and S5B). Two minima at 208 and 222 nm appeared in the CD spectra, as expected for a protein with dominant α-helical structure. Unlike proteins with α-helical structure, the CD spectra of opsin in a hydrophobic environment of both bicelles and micelles showed that the band at 222 nm has larger absolute molar ellipticity values than the band at 208 nm. Indeed, this spectral characterization has been observed for rod and cone outer segment opsins [52]. Isolated, hydrated α-helix structures show the molar ellipticity ratio $[\theta]_{222}/[\theta]_{208} \approx 0.85$ [53], while coiled-coil motifs display increased values around 1.02 [54–57]. When opsin was reconstituted in bicelles, CD spectra showed the $[\theta]_{222}/[\theta]_{208}$ of 1.18 ± 0.01, while in the DDM-solubilized counterpart equaled 1.10 ± 0.02 (Table 1 and Fig. S5C and S5D). This result suggests that other helical arrangements, such as tighter helix-helix interactions or 3_{10} helices, contribute to the structure of opsin embedded into its native lipid (hydrophobic) environment.

The analysis of the CD spectra indicated a significant contribution of increased inter-helical contacts to the overall α-helical content. According to X-ray diffraction data, rhodopsin has a predominantly α-helical structure, with approximately 55% - 63% of its secondary structure consisting of α-helices [3,58,59]. These helices are bent, and some segments adopt a 3_{10}-helical conformation [6]. The remaining structure comprises random coils in the extracellular and intracellular domains, along with a small proportion of *β*-sheets, as determined from its crystal structure [3].

To get more detailed information about the secondary structure composition of opsin in bicelles, the IR spectrum in the amide mode absorption region in D_2O solution was recorded, as shown in Fig. 4B. The secondary structure composition of the protein was quantified by deconvoluting the amide I′ region of the spectrum (1700–1600 cm^{-1}, with band positions identified via the second derivative analysis (Fig. 4B). The strongest and broadest (fwhm = 25 cm^{-1}) amide I′ absorption band centered at 1656 cm^{-1} corresponds to α-helices. This dominant secondary structure element accounts for 48% of opsin composition and is comparable to the content of α-helices reported for rhodopsin in disc membrane [60]. These other helical/random coil structures, assigned to the amide I′ band centered at 1640 cm^{-1}, consist of ca. 15% of secondary structure elements in opsin. The bands at 1628 cm^{-1} and 1687 cm^{-1} are attributed to *β*-sheets, while the band at 1675 cm^{-1} corresponds to *β*-turns. Random coils may also give amid I′ mode around 1630 cm^{-1} as well as 1670–1680 cm^{-1}, complicating quantitative secondary element structure analysis.

Table 1
The molar ellipticity $[\theta]_{222}/[\theta]_{208}$ ratios of bleached rhodopsin (opsin) in DMPC/DHPC bicelles and DDM micelles, obtained from three independent CD measurements. They suggest a significantly tighter packing (one-tailed *t*-test, *p*-value = 0.002) of the helices.

	$[\theta]_{222}/[\theta]_{208}$				
Aggregate from	Run I	Run II	Run III	Avg	SD
opsin in bicelles	1.17	1.19	1.18	1.18	0.01
opsin in DDM	1.11	1.12	1.08	1.10	0.02

one-tailed t-test.
p-value = 0.002.

2.4. Thermal stability of opsin in bicelles

Thermal stability of opsin in bicelles was studied in comparison to the sample in the detergent environment (DDM) by means of CD

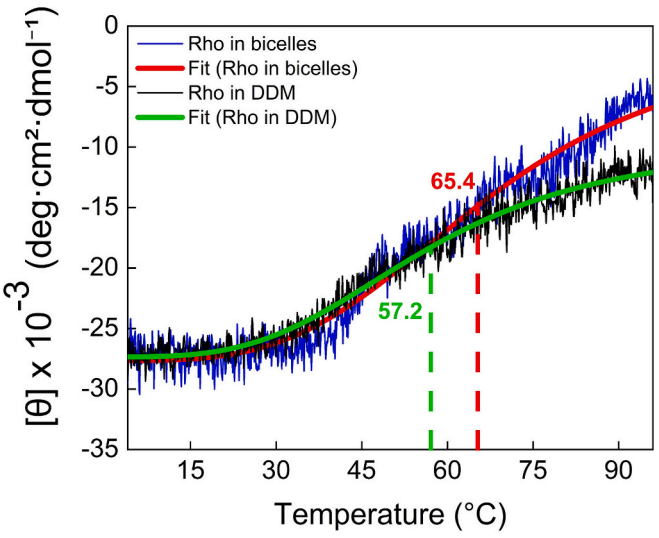

Fig. 5. Temperature-dependent recordings compare changes in the ellipticity of opsin (Rho) in bicelles with opsin in DDM. Representative thermal unfolding profiles were monitored at 208 nm. Data fitting to a 4-parameter Hill sigmoidal function ($R = 0.941$ for opsin in bicelles; $R = 0.987$ for opsin in DDM).

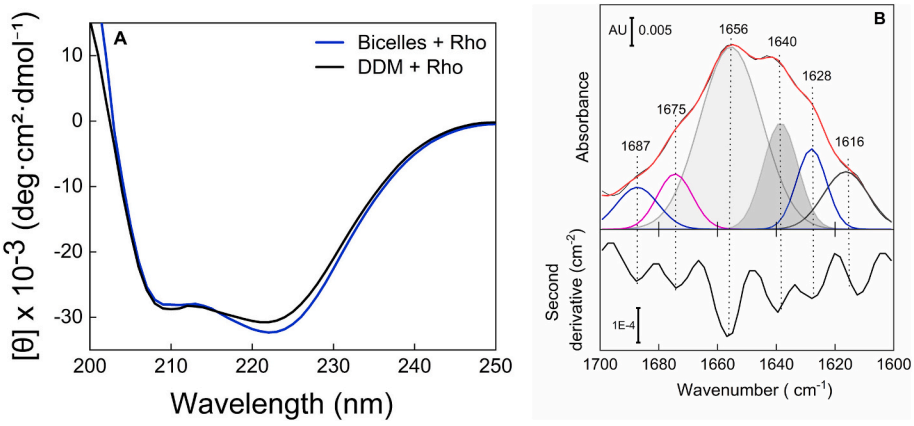

Fig. 4. Spectroscopic characterization of bleached rhodopsin in bicelles and DDM. (A) Far-UV CD spectra of WT bleached rhodopsin in bicelles (blue) or DDM (black). Spectra show the average obtained from three independent samples of each type (6 μM rhodopsin in bicelles (14 mM total lipid concentration). (B) Deconvoluted IR spectrum of the amide I′ region (1700–1600 cm^{-1}) of bleached rhodopsin in bicelles, recorded in phosphate buffer in D_2O (pD = 7.6), with Gaussian fitting applied and second derivative above. Black line – experimentally measured spectrum, red line – fitted sum of Gaussian functions. Grey band – $\upsilon_{as}CO^-$ from side chains, dark blue – *β*-sheets, greyed out bands – α-helix (light grey) and coiled-coils (dark grey), pink – *β*-turns.

spectroscopy (Fig. 5). All samples were bleached prior to measurement and were not dark-adapted. The molar ellipticity at 208 nm, characteristic of the α-helical structure, was measured over the temperature range of 4–96 °C. A decrease in ellipticity as a function of the increase in temperature indicates a loss of α-helical structure of opsin (Fig. 5). The experimental data were fitted to a 4-parameter Hill sigmoidal function, see eq. 1 in the experimental section, as shown in Fig. 5. The thermal profiles of opsin exhibited an inflection point representing the melting temperature (T_m) at 65.4 ± 1.5 °C (n = 3) when embedded in bicelles and at 57.2 ± 2.0 °C (n = 3) in the presence of DDM, indicating that bicelles increase opsin's stability. Moreover, the estimated T_m values for opsin in bicelles (Section S7a, Table S5) showed lower standard deviation compared to the protein sample in DDM, suggesting higher thermal stability and lower experimental variability. A t-test (Section S7, Table S6) comparing the mean T_m values indicated the difference between the bicelles and DDM being statistically significant ($p < 0.05$), which supports the conclusion that opsin is more thermally stable in bicelles.

We further compared the thermostability of DDM micelles and bicelles by DLS measurements at increasing temperatures between 20 and 90 °C showing that bicelles maintained a nearly constant hydrodynamic diameter of ~10–13 nm over the entire temperature range. In contrast, DDM micelles exhibited a narrow stability window limited to 25–35 °C, where hydrodynamic diameters ranged from 47 to 72 nm with low polydispersity (PDI = 0.19–0.23 ± 0.01–0.05). Above 40 °C, *Z*-Average increased sharply to 139–329 nm (PDI = 0.25–0.29), followed by massive aggregation exceeding 400 nm at 55 °C and reaching 2294 ± 790 nm at 85 °C (PDI = 0.82 ± 0.16). See Figs. S6 A to S6C and an extended experimental description in paragraph S7b.

2.5. Immobilization of rhodopsin in bicelles on sensor surfaces

Dark-adapted rhodopsin in detergent/micelle preparations can be captured on dextran-coated SPR sensor chips using immobilized ConA as a binding ligand [18,61–63]. The immobilization density of ConA was very similar, reaching 2498 ± 360 RU, corresponding to 5.35 × 10^{10} monomers per mm^2. We applied this experimental approach to test whether and how rhodopsin in bicelles can be anchored to functionalized surfaces. Rhodopsin solubilized in 3-[(3-cholamidopropyl)dimethylammonium]-1-propanesulfonate (CHAPS) was used as a control, as it was previously documented by Komolov et al. [62] as the most effective medium for subsequent protein-protein interaction studies (e.g. rhodopsin-G_t). Fig. 6A shows the immobilization of rhodopsin in three different lipophilic media: CHAPS, DDM, and bicelles. After washing with a buffer of unspecifically adsorbed protein, rhodopsin in CHAPS reached 5236 RU and in DDM about 2500 RU on average (1800 RU in Fig. 6A), corresponding to 125 fmol/mm^2 and 63 fmol/mm^2, respectively, in agreement with previous results [18,61–63]. SPR curve of

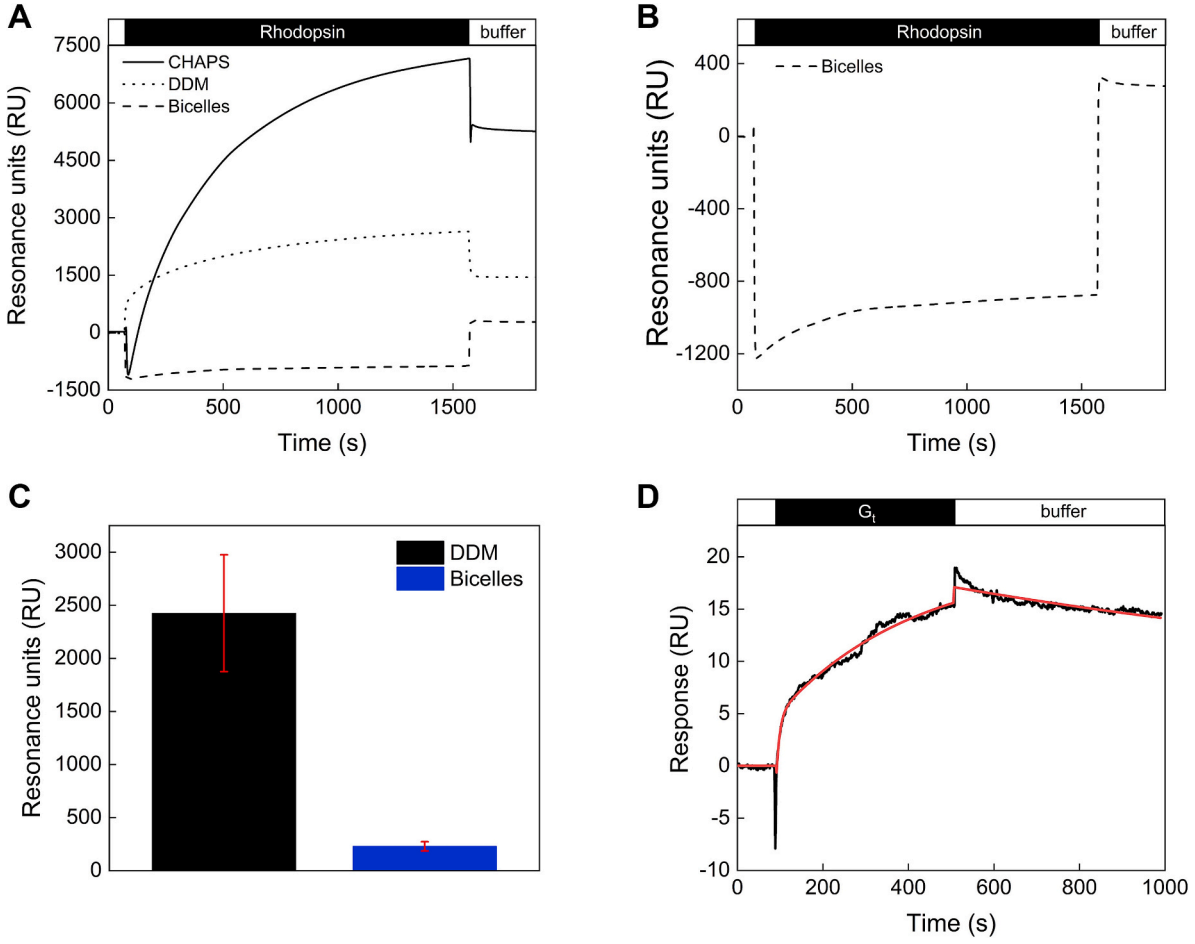

Fig. 6. Immobilization of rhodopsin on ConA-coated sensor chips and interaction study. (A) Rhodopsin in CHAPS, DDM, and bicelles was flushed over a ConA-coated CM5 sensor chip. The black bar indicates the time of injection, and open bars represent buffer flow. (B) Rhodopsin in bicelles flushed over a ConA-coated CM5 sensor chip. (C) Comparison of immobilization levels of rhodopsin in DDM (2425 RU ± 550 RU) and in bicelles (229 RU ± 43 RU) as indicated (n = 6). (D) Purified G_t at 1 μM was injected into the buffer flow during the time indicated by the black bar, resulting in the displayed sensorgram (black trace). Two-state reaction model gave the following parameters: k_a^1 = 2.49 × 10^3 (M^{-1} s^{-1}), k_d^1 = 6.11 × 10^{-4} (s^{-1}), k_a^2 = 9.48 × 10^4 (M^{-1} s^{-1}), k_d^2 = 1.46 × 10^{-7} (s^{-1}), $Rmax^1$ = 18.6 RU, $Rmax^2$ = 6.08 RU.

bicelles containing rhodopsin (Fig. 6A and B) displays a decrease in resonance units during their interactions with the ConA-modified SPR sensor. The drop in RU to negative values is likely due to a change in bulk refractive index between buffer composition and bicelles. Micelles formed during spreading of the DMPC-rhodopsin bilayer on the ConA-coated surface. Free bicelles are found above a bilayer surface in a different system [64] and are washed away by the buffer. The same phenomenon might have occurred in our system leading to a final increase of RU to positive values. Compared to CHAPS and DDM micelles, the increase in RU is small, reaching only 229 RU ± 43 (Fig. 6A, B, C), indicating an increase in mass of 229 pg mm^{-2}. Since only bicelles with incorporated rhodopsin were attached to the sensor chip surface via ConA binding, we calculated that 7.3% or 16.7 pg mm^{-2} of the mass corresponded to rhodopsin. (details of the calculation are described in Section S5b). Thus, the protein concentration on the sensor surface equaled 0.42 fmol mm^{-2} or 2.5 × 10^8 molecules per mm^2.

In a subsequent binding study, we tested the binding of purified native G_t (SDS-PAGE analysis in Section S8, Fig. S7) to immobilized rhodopsin embedded in bicelles. One example of the binding signal is shown in Fig. 6D. Evaluation of several recordings yielded a mean RU amplitude of 28 ± 22 ($n = 4$) corresponding to 4.3 × 10^8 molecules of G_t per mm^2.

3. Discussion

In our study, $DMPC_{(core)}/DHPC_{(rim)}$ bicelles were prepared with a q-value of 0.5. The concerted use of TEM, FCS, and DLS techniques confirmed a flattened ellipsoid shape and uniform size distribution of the lipid bicelles. The size analysis revealed that the bicelles had an average diameter of 11.6 ± 0.6 nm (DLS) and 10.5 nm (TEM, FCS), and the DMPC bilayer core thickness of 4.4 ± 0.5 nm (TEM). Our results align well with the values reported by McKibbin et al. [42] and Kaya et al. [33]. It is worth noting that freezing and thawing cycles do not affect the size and stability of the pure lipid bicelles. Instead, bicelles solutions that are unstable for longer times under room temperature can be stored frozen for longer times.

DLS results showed that after incorporation of rhodopsin, the average diameter of the bicelles increased to 14.9 ± 0.6 nm, see Fig. 3. This increase in size by 3–4 nm correlates with the dimensions of the membrane-inserted part of rhodopsin, 2.8 × 3.9 nm, while the protein height equals 6.4 nm [65], suggesting that one rhodopsin molecule is incorporated into a bicelle. Theoretical and experimental studies have shown that the ideal hydrophobic thickness of rhodopsin is 2.7 ± 0.1 nm [66–68]. The DMPC core bilayer thickness is close to 4.4 ± 0.5 nm. After subtracting 1.6 nm to account for the phosphatidylcholine headgroup regions on both sides of the bilayer [69,70] the remaining 2.8 nm corresponds to the thickness of the hydrophobic hydrocarbon core. This value matches perfectly with the hydrophobic part of the TMP. Consequently, the C- and N-termini of rhodopsin extend on each side by ca. 1 nm above the DMPC core bilayer surface. However, freezing and thawing cycles showed an increase in the average size of bicelles to 17.2 ± 1.4 nm, indicating clustering or agglomeration, pointing to the rhodopsin's property to form oligomers in the lipid environment [66,71,72].

Although the higher A_{280}/A_{500} ratio (3.3 ± 0.7) that we calculated from UV–vis spectra of samples of bicelles with rhodopsin (Fig. 2B) could at first suggest that protein incorporation into lipid particles causes partial bleaching of rhodopsin, our data does not support this interpretation (see Fig. 2B). If the reconstitution of rhodopsin in a bicellar environment were responsible for such bleaching, keeping at the same time dark conditions, a pronounced absorbance band characteristic of all-trans retinal would be prominent near 380 nm [46]. Instead, only a weak peak is observed around this wavelength, indicating that most rhodopsin molecules remained in the dark-adapted state after reconstitution. Therefore, the increase in the A_{280}/A_{500} ratio likely reflects minor bleaching from sample handling or brief dim light exposure. Furthermore, similar preparations of rhodopsin in DDM micelles yielded an A_{280}/A_{500} ratio of 2.5 (Fig. 2B), indicating a strong influence of the apolar versus more polar environment on the absorbance properties of aromatic side chains in rhodopsin. Wild-type rhodopsin in micelles showed the A_{280}/A_{500} ratio in the range of 1.6–2.4, being similar to our results. Variations of the A_{280}/A_{500} ratio in wildtype rhodopsin have been reported in the literature with values reaching 2.4 and more, but these were mainly explained by contaminations or protein aggregates [1]. However, according to our SDS-PAGE analysis the rhodopsin sample in bicelles contained no visible protein contaminants (Fig. 2A).

Opsin embedded in the bicelle structure retains predominant helical secondary structure of dark-adapted rhodopsin, as confirmed by CD and IR spectroscopies (Fig. 4). The CD spectrum, in the 200–250 nm, displays two molar ellipticity minima at 208 and 222 nm, confirming that helical structures are the dominant secondary structure element of rhodopsin. Similarly, deconvolution of the amide I′ band of the IR spectrum of bicelles with opsin in the D_2O phosphate buffer solution gives the strongest absorption band at 1656 cm^{-1}, confirming that α-helices are the main component of rhodopsin's structure [52]. However, non-typically for a protein with α-helical structure, the band at 222 nm has a higher absolute value of the molar ellipticity than the band at 208 nm, indicating either some conformational changes in the helices of the membrane protein or changes in their packing [52,73]. For the opsin embedded in bicelles, the $[\theta]_{222}/[\theta]_{208}$ ratio equals 1.18 ± 0.01 and is comparable to CD spectra recorded by Liu et al. [52] for rhodopsin solubilized in DDM. The $[\theta]_{222}/[\theta]_{208}$ ratio > 1 is an indicator for the formation of coiled-coil helices [54,55]. The presence of the deconvoluted amide I′ mode at 1639 cm^{-1} may indeed support this finding. However, Garcia-Quintana et al. [60] assigned the amide I′ mode at 1639 cm^{-1} to the presence of 3_{10}-helices in rhodopsin within rod disc membranes. In literature, the amide I′ mode assigned to 3_{10}-helices is centered either around 1660–70 cm^{-1} [74,75] or around 1640–30 cm^{-1} [58,76]. In the 3_{10}-helix, the ψ torsion angle undergoes fluctuations depending on the polarity of the surrounding medium [60], reflecting its conformational instability in polar medium (water). In a non-polar medium, the 3_{10}-helix conformation is more stable. The $CO^{\cdots}H_2N$ hydrogen bonds occur between every third amino acid, while in the α-helix, every fourth amino acid is involved in the formation of hydrogen bonds. The average length of the hydrogen bond in the 3_{10}-helix varies between 2.4 and 2.7 Å, going from non-polar to polar media, while in the α-helix its length is close to 2.1–2.2 Å and does not depend on the solvent polarity. Considering longer and therefore weaker hydrogen bonds between the amino acids at the 3_{10}-helix, its amide I′ mode is expected at higher wavenumbers compared to the α-helix. Since the 3_{10}-helix is more tightly wound, longer, and thinner, the hydrogen bond network in the helix will change in water since the water molecules will hydrate it [60,77]. Thus, in a polar environment, a down-shift of the amide I′ mode of a 3_{10}-helix below the expected maximum of absorption of the amide I′ mode of α-helices may occur, complicating the assignment of the deconvoluted amide I′ mode. Interestingly, the CD spectra show that in a protein with 3_{10}-helices the $[\theta]_{222}/[\theta]_{208}$ ratio drastically changes and is close to 0.4 [73,78]. Taken together, in our case 3_{10}-helices do not contribute to the opsin structure. Based on the analysis of the CD and IR spectra described above, the amide I′ mode in opsin embedded into bicelles pointed to a tighter helix-helix interactions. Hydrophobic amino acids seem to be essential for folding into coiled coils [79], and indeed the primary structure of rhodopsin is dominated by hydrophobic residues [6]. In addition, the hydrophobic environment of the lipid bilayer may enhance the interactions between the hydrophobic amino acids, facilitating the stabilization of the enhanced α-helical packing.

Circular dichroism (CD) measurements at 208 nm were also used to determine the melting temperature (T_m) of bleached rhodopsin incorporated into bicelles and, for comparison, in a detergent environment (DDM) over a temperature range of 4 °C to 96 °C (Fig. 5). Previous studies reported T_m values of 71.9 ± 0.4 °C for dark-adapted rhodopsin in rod outer segments and 55.9 ± 0.4 °C for the bleached form (opsin),

indicating that the bleached state is thermally less stable [80,81]. In our experiments, bleached rhodopsin incorporated into bicelles exhibited T_m of 65.4 ± 1.5 °C, suggesting that the bicellar environment enhances thermal stability relative to detergent micelles. Bicelles without opsin maintain a constant hydrodynamic diameter over a large temperature range, which confirms that the denaturation of bleached rhodopsin is not due to the disintegration of bicelles (Fig. S6). This stabilization likely results from the more compact and membrane-like organization imposed by bicelles, which promotes tighter helix-helix interactions within the protein (Fig. 4). Such interactions reduce solvent exposure of hydrophobic residues and strengthen intramolecular packing, thereby increasing resistance to thermal unfolding [82,83]. Schneider et al. [84] showed that helix-helix contacts significantly contribute to the stability of membrane proteins, which may explain the higher T_m observed for opsin in bicelles. The lipid bilayer environment can also alter the denaturation temperature of rhodopsin [85,86], supporting our conclusion that bicelles serve as an effective membrane-mimetic medium for maintaining native-like structural stability. Concluding, opsin in a bicelle has a structure and conformation comparable to those found in rod outer segment membranes [1,52].

In addition, bicelles also provide a suitable platform for the interaction processes of rhodopsin. Arrestin-1 loses its native structure in the presence of detergent micelles, but bicelles prevent the denaturation of arrestin-1 allowing complex formation with light-activated (phosphorylated) rhodopsin [87,88]. Therefore, we tested the interaction of rhodopsin in bicelles by SPR. Anchoring of dark-adapted rhodopsin on surface-functionalized sensor chips has been a straightforward approach to study protein-protein interaction processes by SPR spectroscopy. Previous attempts used rhodopsin preparations in detergent-lipid mixed micelles for immobilization on sensor chips [18,61–63]. Rhodopsin was not embedded in a bilayer in these previous studies, but was nearly stripped off from lipids and detergents, leaving a small ring of hydrophobic molecules around the transmembrane helix part [18]. However, protein interaction studies with purified G_t revealed kinetic binding data consistent with data obtained by other biophysical methods [24,33,48,89]. In the present work, we extended those studies by testing how bicelles might be used in surface-anchored protein-protein interaction studies. One unexpected result was the low immobilization level of bicelles with rhodopsin on the sensor chip surface (Fig. 6). Given that the mass concentration of rhodopsin in bicelles is approximately 7.3%, ConA captured about 0.42 fmol×mm^{-2}, corresponding to 2.5 × 10^8 rhodopsin molecules per mm^2. This value is close to the number 4.3 × 10^8 G_t molecules as calculated from the binding signal amplitudes (see above), and nearly identical to the lower value of the range 2.3 × 10^8–9.4 × 10^8 that we measured. We conclude that rhodopsin and G_t form a 1:1 complex, leaving some G_t molecules free. An acceptable fit of the binding curve in Fig. 6D was only obtained by applying the *heterogeneous ligand two-state reaction* model of the BIAevaluation software. Heterogeneity of the ligand is a reasonable assumption because we have two components on the sensor chip surface, rhodopsin and the lipid bilayer. Therefore, assuming that the majority of G_t is bound to rhodopsin, the affinity (K_D value) relates to $k_d^1/k_a^1 = 249$ nM. This value is similar to 360 nM for dark-adapted rhodopsin reported previously [18]. Finally, our results of a 1:1 stoichiometry for rhodopsin and G_t showed that all rhodopsin molecules have a uniform orientation and expose their cytoplasmic regions, making them accessible for protein-protein interactions. Our results further point to a monolamellar orientation of bicelles on the sensor chip surface.

In the present study, we provide a comprehensive characterization of bicelles with respect to size, size with an incorporated transmembrane protein, stability and influence on the protein structure, making bicelles a valuable tool for IR and CD spectroscopy studies. By applying both methods, we observed enhanced α-helical packing stabilized by a native-like lipid bilayer.

4. Materials and methods

4.1. Chemicals

1,2-dimyristoyl-sn-glycero-3-phosphocholine (DMPC) (14:0–14:0) and 1,2-diheptanoyl-sn-glycero-3-phosphocholine (DHPC) were purchased from Avanti Polar Lipids, USA. Deuterium oxide (D_2O) was purchased from Deutero, Germany. Anhydrous K_2HPO_4 and K_2HPO_4 and 9,10-bis(phenylethinyl)-anthracene (BPEA) were purchased from Sigma-Aldrich (Germany). HCl (25%), ethanol, and methanol (analytical grade) were from AnalaR Normapur, VWR, France. All aqueous solutions were prepared using freshly filtered water of conductivity ≤0.50 μS cm^{-1} (PureLab Classic, Elga LabWater, Celle, Germany). Concanavalin A (ConA), an affinity chromatography resin, and a CM5 Biacore chip were purchased from Cytiva Europe GmbH, Germany. n-dodecyl-β-D-Maltoside (DDM), methyl-α-D-mannopyranoside, sodium dodecyl sulfate (SDS) pellets, 3-(N-morpholino) propanesulfonic acid (MOPS) and n-octyl-β-D-glucopyranoside (OGP) were from Carl Roth, Germany. ConA and coupling reagents were purchased from Sigma-Aldrich (Cat. No. 11028–71-0, USA). The Bradford reagent for the determination of protein concentration was from Bio-Rad (Hercules, USA). Brilliant Blue R250 was from Serva (Germany).

4.2. Preparation of bicelles

Bicelles were prepared based on the previously described method by Dong et al. [1] For the preparation of 0.4 mL of bicelles, lipids in powder form (22.59 mg of DMPC and 32.10 mg of DHPC) were first dissolved in phosphate buffer (K_2HPO_4/KH_2PO_4, pH 7.2) using 0.25 mL and 0.15 mL of buffer, respectively. The resulting milky DMPC solution was vortexed and incubated on a thermomixer at 42 °C for 5 min. DHPC solution was then added, gently mixed, and incubated at 42 °C for an additional 10 min. The final mixture, with a lipid molar ratio of $q = 0.5$ and a total lipid concentration of 250 mM (corresponding to 12% *w*/w), was then stirred at room temperature for 1 h until it became clear. The resulting bicelles remained stable for up to 48 h in the refrigerator and could be stored at −20 °C after freezing in liquid nitrogen.

4.3. Transmission electron microscopy (TEM)

TEM imaging was performed using a JEOL JEM-2100F instrument with a field emission gun operated at an acceleration voltage of 200 kV. A Gatan Orius SC600CCD camera was used for image acquisition. Prior to sample deposition, pioloform-coated copper grids (3.05 mm, 200 mesh; Plano GmbH, Germany) were washed with ethanol and treated in an ozone chamber for 10 min to remove any organic contaminants. A drop of the bicelle solution at a total lipid concentration equal to either 25 mM or 2.5 mM was deposited onto pioloform-coated copper grid and allowed to dry for one hour. Samples were prepared using negative staining with 1% uranyl acetate (Sigma Aldrich, Germany). After incubation for 30 min, grids were gently washed in a droplet of distilled water and subsequently imaged. ImageJ 1.51w software (University of Wisconsin, USA) was used to analyze the size of the bicelles on the TEM grid. The average diameter and height were obtained by a manual measurement of 15 random bicelles from a sample diluted to 25 mM.

4.4. Dynamic light scattering (DLS)

DLS measurements were performed using a Zetasizer Nano ZS instrument (Malvern Instruments, UK) equipped with a 633 nm laser. The temperature was maintained at 20 °C throughout the measurements. Bicelle samples, both with and without rhodopsin, were diluted to lipid concentrations ranging from 50 mM to 17 mM and analyzed in UV-transparent disposable cuvettes with a 1 cm path length. Prior to each measurement, samples were equilibrated at the set temperature for 2 min to ensure stability. Each experiment consisted of at least 12

individual measurements, which were averaged to obtain reliable size distribution data. The analysis was conducted using Zetasizer Software v7.13. The dispersant refractive index and viscosity were set to 1.33 and 0.89 cP, respectively. The material refractive index was set to 1.45, with an absorption value of 0.001.

4.5. Fluorescence correlation spectroscopy (FCS)

The FCS measurements were performed on a standard FCS setup described in detail in [90]. For time-resolved fluorescence anisotropy, the setup has been upgraded with a polarizing filter between the supercontinuum source and the dichroic mirror, and two polarizing filters in front of the single-photon avalanche photodiode (SPAD) detectors. The supercontinuum source has been operated at an emission wavelength of 470 nm and a 4.8 MHz repetition rate. Data processing has been performed with the Burst Analyzer 2 software (Becker&Hickl, Germany). Bicelles were fluorescently labeled by incorporating BPEA, a membrane-intercalating lipophilic fluorophore well-suited for studying membrane dynamics. Labeling was achieved by adding a 50 mM stock solution of bicelles to dried BPEA, previously dissolved in chloroform. The mixture was gently stirred overnight at room temperature to ensure uniform dye incorporation. For fluorescence anisotropy measurements, the total lipid concentration was adjusted to 25 mM, while $q = 0.5$. For FCS, this solution was diluted with a 25 mM solution of not labeled bicelles to a final BPEA concentration of 1.5 nM. Dilution with label-free bicelle solution ensured that the lipid concentration was above the critical micelle concentration.

4.6. Purification of rhodopsin and Gt

Native proteins were obtained from bovine rod outer segments (ROS) that were either prepared according to [91] or purchased from InVision BioResources (USA). Rhodopsin was isolated from hypotonically stripped disc membranes under dim red light according to [33]. Initially, ROS membranes were washed three times with GTP buffer consisting of 0.1 mM GTP in buffer A (10 mM Tris/HCl, pH 7.4, 0.5 mM $MgCl_2$, 1 mM DTT, 0.1 mM PMSF, 1:500 mPIC) and centrifuged at 120000 x*g* for 5 min at 4 °C. The resulting pellet was resuspended in urea buffer composed of 5 M urea in buffer A and incubated on ice for 10 min, followed by another centrifugation under the same conditions. Obtained pellet was resuspended in buffer B consisting of 10 mM Tris/HCl, pH 7.4, 0.1 M NaCl, 5 mM $MgCl_2$, 1 mM DTT, and 0.1 mM PMSF and washed twice. Subsequently, the pellet was washed two times with EDTA buffer containing 10 mM Tris/HCl, pH 7.5, 1 mM EDTA, 1 mM DTT and centrifuged for 15 min at 120000 x*g* at 4 °C. Finally, the ROS membrane pellet was solubilized in a solubilization buffer composed of 50 mM Tris/HCl, pH 7.5, 100 mM NaCl, and 20 mM DDM and incubated on a thermomixer at 4 °C for 20 min. To eliminate insoluble material, the sample was subjected to a final centrifugation step at 120000 x*g* for 15 min at 4 °C. The G-protein transducin (G_t) was purified as described [18], SDS-PAGE analysis in Section S8, Fig. S6. To obtain G_t in the most suitable conditions for interaction studies, the buffer was exchanged to the SPR running buffer [18], using an NAP™-5 column (Cytiva, USA). The protein concentration was quantified using the Bradford assay [92] and confirmed by UV–Visible spectroscopy. To assess rhodopsin concentration in lipid-containing samples, the Bradford assay with OGP was used. The purity of the samples was evaluated by SDS polyacrylamide gel electrophoresis (PAGE) using a 10% polyacrylamide gel.

4.7. Incorporation of rhodopsin into bicelles

This procedure was conducted under both dim red light and ambient light conditions according to [33], depending on the protein's state. Initially, the ConA affinity column was equilibrated with ten column volumes of binding buffer consisting of 20 mM Tris/HCl, pH 7.4, 1 mM $MgCl_2$, 1 mM $CaCl_2$, 1 mM $MnCl_2$, 200 mM NaCl, 1 mM DTT, and 0.5 mM DDM. DDM-solubilized rhodopsin was applied to the column and incubated on the rotating platform overnight at 4 °C to facilitate efficient binding to ConA. The following day, the unbound fraction was collected, and the column was washed with washing buffer containing competing sugar and 50 mM bicelles made up of 20 mM Tris/HCl, pH 7.4, 100 mM NaCl, 500 mM methyl-α-D-mannopyranoside, which promotes the encapsulation of rhodopsin. This step was followed by 3 h incubation at 4 °C on a rotating platform. Finally, the fraction containing rhodopsin incorporated into bicelles was eluted and subjected to further analysis. For IR, CD, EM, FCS, and SDS-PAGE analyses, rhodopsin in bicelles was bleached prior to measurements, whereas for SPR and UV–Vis spectroscopy, dark-adapted samples were used.

4.8. Light-triggered activation of Gt

Activation of Gt was measured by a tryptophan fluorescence assay similar to previous reports [33,48] with some modifications. Briefly, bicelles containing 220 nM rhodopsin were mixed with 150 nM freshly purified native Gt under dark conditions in a buffer containing 10 mM Tris pH 7.5, 100 mM NaCl, 5 mM $MgCl_2$, 0.1 mM EDTA, 2 mM DTT, 0.006% (*w/v*) DDM, 1 μM GDP and 10 μM GTPγS. Fluorescence emission was recorded at 345 nm by setting the excitation to 300 nm in a spectrofluorimeter from Photon Technology International. The exchange of GDP to GTPγS in Gt was triggered by bleaching rhodopsin in the mixture with white light for 30 s.

4.9. SDS-PAGE analysis of the proteins

SDS-PAGE was performed using a 5% polyacrylamide stacking and 10% resolving gel. The protein bands were visualized by incubating the gel in Coomassie staining solution for a minimum of 30 min under continuous shaking. Afterwards, the gel was washed with a destaining solution until the protein bands were visible over the clear background. The results were captured by the Azure 400 Visible Fluorescent Western System.

4.10. UV–visible absorption

To determine the dark state of rhodopsin in bicelles, UV–vis spectra were acquired with a SPECORD 200 Double Beam spectrophotometer (Analytik Jena, Germany). The spectra were recorded in the range 260–650 nm with a bandwidth of 2 nm, a response time of 0.5 s, and a scan speed of 2 nm s^{-1}. The rhodopsin concentration was determined according to Lambert-Beer law by measuring the absorbance at 280 nm and 500 nm and applying the respective extinction coefficients (ε_{280} = 61,800 cm^{-1} M^{-1} and ε_{500} = 42,000 cm^{-1} M^{-1}) [45,47,48,61].

4.11. Transmission IR spectroscopy

Bicelles with inserted opsin were freshly prepared consisting of a total lipid concentration of 57 mM in phosphate buffer in D_2O at pD 7.6 (background) and opsin concentration of 14.5 ± 2.8 μM ($n = 5$) as analyte. The IR transmission spectra of these bicelles were recorded in a flow cell between two ZnSe windows (Aldrich, Germany) and a 50 μm thick Teflon spacer at room temperature. A Vertex 70 IR spectrometer (Bruker, Germany) was used to record 64 spectra with a resolution of 4 cm^{-1} for the background and analyte spectra.

4.12. Circular dichroism spectroscopy (CDS)

CD spectra were recorded in the far-UV (200–250 nm) to analyze the secondary structure of rhodopsin inserted into bicelles. The spectra were recorded on a Jasco (Japan) J-710 spectropolarimeter equipped with a Peltier-type cell holder in a 0.1 cm path length quartz cuvette with the following parameters: 1 nm bandwidth, 1 nm data pitch, 4 s integration time, 50 nm min^{-1} scanning speed, 20 °C temperature, 3 accumulations.

The far-UV CD spectrum of an 18-fold dilution of the bicelles stock was considered as a blank and subtracted from the spectrum of 6 μM bicelles-reconstituted rhodopsin. Thermal denaturation profiles of rhodopsin in bicelles or DDM were collected by monitoring the ellipticity at 208 nm between 4 °C and 96 °C at 1.5 °C min^{-1} under the same experimental conditions as for far-UV spectra. CD spectra and thermal denaturation profiles were analyzed using JASCO Spectra Manager 1.53.04. Melting profile curves were analyzed using eq. 1:

$$f = y_0 + ax^b/(c^b + x^b) \quad (1)$$

representing a sigmoidal Hill model containing 4 parameters; where y_0 is the baseline signal of the native folded state, *a* represents the amplitude of the unfolding transition, *b* is the Hill coefficient indicating cooperativity, and *c* corresponds to the melting temperature (T_m), the midpoint of the unfolding transition [93,94].

4.13. Surface plasmon resonance (SPR)

SPR measurements were conducted using the Biacore 3000 system (GE Healthcare, now Cytiva, USA) with a CM5 sensor chip. The analysis was performed according to the step-by-step procedure described in [63]. The SPR running buffer consisted of 50 mM MOPS pH 7.5, 150 mM NaCl, 3 mM $MgSO_4$ and 10 μM $CaCl_2$ as described in [18]. All solutions were filtered before use in SPR experiments through 0.22 μm filter. SPR experiments aimed at immobilizing rhodopsin in detergent or bicelle preparations via binding to ConA. The dextran matrix of the CM5 sensor chip was first activated by 35 μL of 50 mM N-hydroxysuccinimide and 200 mM N-ethyl-N′-[(dimethylamino)propyl] carbodiimide at a flow rate of 5 μL/min. The carboxy-activated dextran on the sensor chip surface was coated with ConA by amine linkage chemistry using 7-min injection of 0.1 mg/ml ConA (diluted in 100 mM sodium acetate, pH 5.0). Remaining reactive carboxy groups were deactivated with a 7-min pulse of 1 M ethanolamine hydrochloride, pH 8.5. Dark-adapted rhodopsin incorporated into bicelles was obtained after elution from the ConA affinity column using bicelles and methyl-α-D-mannopyranoside, following a 3-h incubation on a rotating platform. Subsequently, the protein in disc-shaped lipids was diluted 20-fold (total bicelles dilution – 100-times) with 50 mM MES buffer pH 6.0, 1 mM $MnCl_2$, and 1 mM $CaCl_2$ to reach a final rhodopsin concentration of 34.4 μg × mL^{-1}. The solution was injected into the system with a flow rate of 2 μL × min^{-1} for 30 min. Immobilization of rhodopsin on the chip via ConA was previously described in [61,62]. Then, the flow cell was rinsed with SPR running buffer to wash off unbound rhodopsin and surplus bicelles. The extended immobilization time and high dilution (100-times) were meant to allow bicelles containing rhodopsin to spread across the chip surface and form a lipid bilayer [64]. Diluting the stock bicelle solution by a factor of 100–200 destabilizes the structure of the aggregate and leads to their spreading to a planar DMPC bilayer while the DPHC micelles remain in the solution phase [64]. Functional tests of rhodopsin on the sensor chip surface involved interaction studies with purified native bovine G_t. G_t at a final concentration of 0.3 or 1 μM was injected into the system with a flow rate of 5 μL min^{-1} for 15 min. A blank sensogram was recorded by injecting only the SPR running buffer into the system (without analyte) and subtracted from the experimental data to remove non-specific signals, such as baseline drifts or bulk refractive index changes, thus allowing the isolation of the specific binding response of rhodopsin in bicelles with G_t. Densities of receptor and analyte binding amounts were calculated using the Biacore relation 1 RU = 1 pg of protein per mm^2. 28 RU corresponds to 18 pg of Gt (molecular mass 39 kDa), or 7.2 × 10^{-16} mol. Multiplying by the Avogadro number yields 4.3 × 10^8 Gt. Association and dissociation rate constants were obtained by applying nonlinear fitting to the primary sensorgram data using BIAevaluation 4.1 version software. Rhodopsin was handled in the dark under dim red light, but we cannot exclude at least partial bleaching due to laboratory conditions.

Abbreviations

AU	absorbance units
BPEA	9,10-bis(phenylethinyl)-anthracene
cP	centipoise
CDS	circular dichroism spectroscopy
CHAPS	3-[(3-cholamidopropyl)dimethylammonium]-1-propanesulfonate
ConA	concanavalin A
D_2O	deuterium oxide
DDM	dodecyl-β-D-maltoside
DHPC	1,2-diheptanoyl-sn-glycero-3-phosphocholine
DLS	dynamic light scattering
DMPC	1,2-dimyristoyl-sn-glycero-3-phosphocholine
DTT	dithiothreitol
EDTA	ethylenediaminetetraacetic acid
FCS	fluorescence correlation spectroscopy
fwhm	full width at half maximum
GPCR	G protein-coupled receptor
GTP	guanosine triphosphate
Gt	G protein transducin
IRS	infrared spectroscopy
LDAO	lauryldimethylamine oxide
MES	2-(N-Morpholino)ethanesulfonic acid
MOPS	3-(N-morpholino)propanesulfonic acid
mPIC	protease inhibitor cocktail
NMR	nuclear magnetic resonance
OGP	n-octyl-β-D-glucopyranoside
PMSF	phenylmethylsulfonyl fluoride
RU	resonance units
Rho	rhodopsin
ROS	rod outer segments
SDS-PAGE	sodium dodecyl sulfate - polyacrylamide gel electrophoresis
SPAD	single-photon avalanche photodiode
SPR	surface plasmon resonance
TEM	transmission electron microscopy
Tm	melting temperature
Tris	tris(hydroxymethyl)aminomethane
TMPs	transmembrane proteins
τRψ	rotational diffusion time
UV–Vis	ultraviolet-visible spectroscopy
υas	asymmetric stretching vibration
Θ	ellipticity

CRediT authorship contribution statement

Patryk Kamil Bielski: Writing – review & editing, Writing – original draft, Methodology, Investigation, Formal analysis, Conceptualization. **Justyna Bożek:** Writing – review & editing, Writing – original draft, Methodology, Investigation, Formal analysis, Conceptualization. **Valerio Marino:** Writing – review & editing, Methodology, Formal analysis. **Daniele Dell'Orco:** Writing – review & editing, Methodology, Formal analysis. **Carsten Dosche:** Writing – review & editing, Methodology. **Izabella Brand:** Writing – review & editing, Supervision, Methodology, Investigation, Funding acquisition, Formal analysis, Conceptualization. **Karl-Wilhelm Koch:** Writing – review & editing, Supervision, Methodology, Investigation, Funding acquisition, Formal analysis, Conceptualization.

Funding sources

We acknowledge financial support from the Deutsche Forschungsgemeinschaft (DFG) to IB (BR 3961/13–1; project number: 510809665) and KWK (KO 948/18–1; project number: 510809665), DFG grant (INST 184/ 106–1 FUGG) (HR TEM). Project „MIX IT" Erasmus+ Traineeships for students/graduates; projekt-code: 2024–1-

DE01-KA131-HED-000220537.

Declaration of competing interest

The authors declare that they have no known competing financial interests or personal relationships that could have appeared to influence the work reported in this paper.

Acknowledgements

The authors acknowledge the Electron and Light Microscopy Service Unit of the School of Mathematics and Science of the Carl von Ossietzky University for the use of the imaging facilities. The authors thank Dr. V. Solovyeva for the performance of the TEM measurements. The Centro Piattaforme Tecnologiche of the University of Verona is acknowledged for providing access to the spectroscopic platforms.

Appendix A. Supplementary data

Supplementary data to this article can be found online at https://doi.org/10.1016/j.bbamem.2026.184528.

Data availability

The data referred to in this manuscript are present in the manuscript and in the supporting information. Unprocessed data are deposited on a server of the University of Oldenburg in accordance with the data policy of the University of Oldenburg and can be made available on request from the corresponding author.

References

[1] X. Dong, et al., Phospholipid Bicelles improve the conformational stability of rhodopsin mutants associated with retinitis Pigmentosa, Biochemistry 54 (31) (2015) 4795–4804.
[2] P.A. Hargrave, J.H. McDowell, Rhodopsin and phototransduction: a model system for G protein-linked receptors, FASEB J. 6 (6) (1992) 2323–2331.
[3] K. Palczewski, et al., Crystal structure of rhodopsin: a G protein-coupled receptor, Science 289 (5480) (2000) 739–745.
[4] J. Standfuss, et al., Crystal structure of a thermally stable rhodopsin mutant, J. Mol. Biol. 372 (5) (2007) 1179–1188.
[5] J. Li, et al., Structure of bovine rhodopsin in a trigonal crystal form, J. Mol. Biol. 343 (5) (2004) 1409–1438.
[6] S. Filipek, et al., G protein-coupled receptor rhodopsin: a prospectus, Annu. Rev. Physiol. 65 (2003) 851–879.
[7] F. DeLange, et al., Probing intramolecular orientations in rhodopsin and Metarhodopsin II by polarized infrared difference spectroscopy, Biochemistry 38 (40) (1999) 13200–13209.
[8] K.J. Rothschild, W.A. Cantore, H. Marrero, Fourier transform infrared difference spectra of intermediates in rhodopsin bleaching, Science 219 (4590) (1983) 1333–1335.
[9] S. Senapati, et al., Differentiating between inactive and active states of rhodopsin by atomic force microscopy in native membranes, Anal. Chem. 91 (11) (2019) 7226–7235.
[10] T.B. Feldman, et al., Small-angle neutron and X-ray scattering analysis of the supramolecular organization of rhodopsin in photoreceptor membrane, Biochim. Biophys. Acta Biomembr. 1861 (10) (2019) 183000.
[11] P.A. Liebman, G. Entine, Lateral diffusion of visual pigment in photorecptor disk membranes, Science 185 (4149) (1974) 457–459.
[12] M. Poo, R.A. Cone, Lateral diffusion of rhodopsin in the photoreceptor membrane, Nature 247 (5441) (1974) 438–441.
[13] D. Fotiadis, et al., Is rhodopsin dimeric in native retinal rods? Nature 426 (6962) (2003) 31.
[14] D. Fotiadis, et al., The G protein-coupled receptor rhodopsin in the native membrane, FEBS Lett. 564 (3) (2004) 281–288.
[15] S. Senapati, P.S. Park, Investigating the Nanodomain Organization of Rhodopsin in native membranes by atomic force microscopy, Methods Mol. Biol. 1886 (2019) 61–74.
[16] M. Gunkel, et al., Higher-order architecture of rhodopsin in intact photoreceptors and its implication for phototransduction kinetics, Structure 23 (4) (2015) 628–638.
[17] P.S. Park, Supramolecular organization of rhodopsin in rod photoreceptor cell membranes, Pflugers Arch. 473 (9) (2021) 1361–1376.
[18] D. Dell'Orco, K.W. Koch, A dynamic scaffolding mechanism for rhodopsin and transducin interaction in vertebrate vision, Biochem. J. 440 (2) (2011) 263–271.
[19] B. Jastrzebska, et al., Role of membrane integrity on G protein-coupled receptors: rhodopsin stability and function, Prog. Lipid Res. 50 (3) (2011) 267–277.
[20] M.L. Jackson, B.J. Litman, Rhodopsin-phospholipid reconstitution by dialysis removal of octyl glucoside, Biochemistry 21 (22) (1982) 5601–5608.
[21] M.R. Whorton, et al., Efficient coupling of transducin to monomeric rhodopsin in a phospholipid bilayer, J. Biol. Chem. 283 (7) (2008) 4387–4394.
[22] O. Soubias, et al., Physiological changes in bilayer thickness induced by cholesterol control GPCR rhodopsin function, Biophys. J. 122 (6) (2023) 973–983.
[23] D.C. Mitchell, S.L. Niu, B.J. Litman, Optimization of receptor-G protein coupling by bilayer lipid composition I: kinetics of rhodopsin-transducin binding, J. Biol. Chem. 276 (46) (2001) 42801–42806.
[24] Z. Salamon, et al., Surface plasmon resonance spectroscopy studies of membrane proteins: transducin binding and activation by rhodopsin monitored in thin membrane films, Biophys. J. 71 (1) (1996) 283–294.
[25] C.R. Sanders, R.S. Prosser, Bicelles: a model membrane system for all seasons? Structure 6 (10) (1998) 1227–1234.
[26] E.F. Kot, et al., Phase transitions in Small isotropic Bicelles, Langmuir 34 (11) (2018) 3426–3437.
[27] K.S. Mineev, et al., Characterization of Small isotropic Bicelles with various compositions, Langmuir 32 (26) (2016) 6624–6637.
[28] K.J. Glover, et al., Structural evaluation of phospholipid bicelles for solution-state studies of membrane-associated biomolecules, Biophys. J. 81 (4) (2001) 2163–2171.
[29] M.N. Triba, D.E. Warschawski, P.F. Devaux, Reinvestigation by phosphorus NMR of lipid distribution in Bicelles, Biophys. J. 88 (3) (2005) 1887–1901.
[30] S. Choi, et al., Continuous preparation of bicelles using hydrodynamic focusing method for bicelle to vesicle transition, Micro and Nano Systems Letters 9 (1) (2021) 7.
[31] U.H.N. Dürr, M. Gildenberg, A. Ramamoorthy, The magic of Bicelles lights up membrane protein structure, Chem. Rev. 112 (11) (2012) 6054–6074.
[32] J.M. Hutchison, et al., Bicelles rich in both sphingolipids and cholesterol and their use in studies of membrane proteins, J. Am. Chem. Soc. 142 (29) (2020) 12715–12729.
[33] A.I. Kaya, et al., Coupling efficiency of rhodopsin and Transducin in Bicelles, Biochemistry 50 (15) (2011) 3193–3203.
[34] R.S. Prosser, et al., Current applications of Bicelles in NMR studies of membrane-associated Amphiphiles and proteins, Biochemistry 45 (28) (2006) 8453–8465.
[35] D. Dziubak, S. Sęk, Sparsely tethered bilayer lipid membranes formed by self-assembly of bicelles: Spectroelectrochemical characterization and incorporation of transmembrane protein, Bioelectrochemistry 153 (2023) 108482.
[36] T.N. Sut, et al., Characterizing the supported lipid membrane formation from cholesterol-rich Bicelles, Langmuir 35 (47) (2019) 15063–15070.
[37] K. Morigaki, et al., Formation of substrate-supported membranes from mixtures of long- and short-chain phospholipids, Langmuir 28 (25) (2012) 9649–9655.
[38] T.N. Sut, et al., Influence of NaCl concentration on Bicelle-mediated SLB formation, Langmuir 35 (32) (2019) 10658–10666.
[39] S.H. Park, et al., High-resolution NMR spectroscopy of a GPCR in aligned Bicelles, J. Am. Chem. Soc. 128 (23) (2006) 7402–7403.
[40] J.B. Brettmann, et al., Role of protein dynamics in ion selectivity and allosteric coupling in the NaK channel, Proc. Natl. Acad. Sci. USA 112 (50) (2015) 15366–15371.
[41] K.R. Vinothkumar, Structure of rhomboid protease in a lipid environment, J. Mol. Biol. 407 (2) (2011) 232–247.
[42] C. McKibbin, et al., Opsin stability and folding: modulation by phospholipid bicelles, J. Mol. Biol. 374 (5) (2007) 1319–1332.
[43] M.J. Janiak, D.M. Small, G.G. Shipley, Temperature and compositional dependence of the structure of hydrated dimyristoyl lecithin, J. Biol. Chem. 254 (13) (1979) 6068–6078.
[44] F. Luschtinetz, C. Dosche, Determination of micelle diffusion coefficients with fluorescence correlation spectroscopy (FCS), J. Colloid Interface Sci. 338 (1) (2009) 312–315.
[45] R. Hubbard, Absorption Spectrum of rhodopsin: 280 nm absorption band, Nature 221 (5179) (1969) 435–437.
[46] B. Jastrzebska, et al., Isolation and functional characterization of a stable complex between photoactivated rhodopsin and the G protein, transducin, FASEB J. 23 (2008) 371–381.
[47] R. Hubbard, Absorption Spectrum of rhodopsin: 500 nm absorption band, Nature 221 (5179) (1969) 432–435.
[48] O.P. Ernst, et al., Monomeric G protein-coupled receptor rhodopsin in solution activates its G protein transducin at the diffusion limit, Proc. Natl. Acad. Sci. USA 104 (26) (2007) 10859–10864.
[49] H. Wu, et al., Assessing the size, stability, and utility of isotropically tumbling bicelle systems for structural biology, Biochim. Biophys. Acta 1798 (3) (2010) 482–488.
[50] J.N. Israelachvili, D.J. Mitchell, A model for the packing of lipids in bilayer membranes, Biochim. Biophys. Acta 389 (1) (1975) 13–19.
[51] M. Mozafari, E. Mazaheri, K. Dormiani, Simple equations pertaining to the particle number and surface area of metallic, polymeric, *Lipidic and Vesicular Nanocarriers*, Sci. Pharm. 89 (2021) 15.
[52] X. Liu, P. Garriga, H.G. Khorana, Structure and function in rhodopsin: correct folding and misfolding in two point mutants in the intradiscal domain of rhodopsin identified in retinitis pigmentosa, Proc. Natl. Acad. Sci. USA 93 (10) (1996) 4554–4559.
[53] R.O. Crooks, T. Rao, J.M. Mason, Truncation, randomization, and selection: generation of a reduced length c-Jun antagonist that retains high interaction stability, J. Biol. Chem. 286 (34) (2011) 29470–29479.

[54] N. Choy, V. Raussens, V. Narayanaswami, Inter-molecular coiled-coil formation in human apolipoprotein E C-terminal domain, J. Mol. Biol. 334 (3) (2003) 527–539.
[55] J.D. Franke, et al., Rod mutations associated with MYH9-related disorders disrupt nonmuscle myosin-IIA assembly, Blood 105 (1) (2005) 161–169.
[56] R.S. Vieira-Pires, J.H. Morais-Cabral, 3(10) helices in channels and other membrane proteins, J. Gen. Physiol. 136 (6) (2010) 585–592.
[57] M.L. Smythe, S.E. Huston, G.R. Marshall, The molten Helix: effects of solvation on the alpha - to 3_{10}-helical transition, J. Am. Chem. Soc. 117 (20) (1995) 5445–5452.
[58] A.M.A. Pistorius, W.J. Degrip, Rhodopsin's secondary structure revisited: assignment of structural elements, Biochem. Biophys. Res. Commun. 198 (3) (1994) 1040–1045.
[59] S. Lindert, et al., EM-fold: De novo folding of α-helical proteins guided by intermediate-resolution Electron microscopy density maps, Structure 17 (7) (2009) 990–1003.
[60] D. Garcia-Quintana, P. Garriga, J. Manyosa, Quantitative characterization of the structure of rhodopsin in disc membrane by means of Fourier transform infrared spectroscopy, J. Biol. Chem. 268 (4) (1993) 2403–2409.
[61] K.E. Komolov, et al., Surface Plasmon resonance study of G protein/receptor coupling in a lipid bilayer-free system, Anal. Chem. 78 (4) (2006) 1228–1234.
[62] K.E. Komolov, et al., On-chip photoactivation of heterologously expressed rhodopsin allows kinetic analysis of G-protein signaling by surface plasmon resonance spectroscopy, Anal. Bioanal. Chem. 397 (7) (2010) 2967–2976.
[63] K.E. Komolov, K.-W. Koch, Application of surface Plasmon resonance spectroscopy to study G-protein coupled receptor Signalling, in: N.J. Mol, M.J.E. Fischer (Eds.), Surface Plasmon Resonance: Methods and Protocols, Humana Press, Totowa, NJ, 2010, pp. 249–260.
[64] J. Bożek, et al., Monitoring of Bicelles spreading into floating lipid bilayers, Langmuir 41 (31) (2025) 20942–20953.
[65] G.F.X. Schertler, P.A. Hargrave, Preparation and Analysis of Two-Dimensional Crystals of Rhodopsin, in: Methods Enzymol, Academic Press, San Diego, CA, 2000, pp. 91–107.
[66] O. Soubias, et al., Rhodopsin/lipid hydrophobic matching-rhodopsin oligomerization and function, Biophys. J. 108 (5) (2015) 1125–1132.
[67] O. Soubias, K. Gawrisch, The role of the lipid matrix for structure and function of the GPCR rhodopsin, Biochim. Biophys. Acta 1818 (2) (2012) 234–240.
[68] A. Grossfield, S.E. Feller, M.C. Pitman, A role for direct interactions in the modulation of rhodopsin by omega-3 polyunsaturated lipids, Proc. Natl. Acad. Sci. USA 103 (13) (2006) 4888–4893.
[69] G. Vancuylenberg, et al., Planar confined water organisation in lipid bilayer stacks of phosphatidylcholine and phosphatidylethanolamine, Soft Matter 19 (27) (2023) 5179–5192.
[70] H.I. Petrache, S. Tristram-Nagle, J.F. Nagle, Fluid phase structure of EPC and DMPC bilayers, Chem. Phys. Lipids 95 (1) (1998) 83–94.
[71] B. Jastrzebska, et al., Functional and structural characterization of rhodopsin oligomers, J. Biol. Chem. 281 (17) (2006) 11917–11922.
[72] A.V. Botelho, et al., Curvature and hydrophobic forces drive oligomerization and modulate activity of rhodopsin in membranes, Biophys. J. 91 (12) (2006) 4464–4477.
[73] G.L. Millhauser, et al., Estimating the relative populations of 3_{10}-helix and α-helix in ala-rich peptides: a hydrogen exchange and high field NMR study, J. Mol. Biol. 267 (4) (1997) 963–974.
[74] S.C. Yasui, et al., Vibrational circular dichroism of polypeptides, V. A study of 3 (10)-helical-octapeptides, Biopolymers 25 (1) (1986) 79–89.
[75] L.K. Tamm, S.A. Tatulian, Infrared spectroscopy of proteins and peptides in lipid bilayers, Q. Rev. Biophys. 30 (4) (1997) 365–429.
[76] C.R. Jacob, S. Luber, M. Reiher, Analysis of secondary structure effects on the IR and Raman spectra of polypeptides in terms of localized vibrations, J. Phys. Chem. B 113 (18) (2009) 6558–6573.
[77] R.B. Nellas, Q.R. Johnson, T. Shen, Solvent-induced α- to 3(10)-helix transition of an amphiphilic peptide, Biochemistry 52 (40) (2013) 7137–7144.
[78] P. Kumar, et al., De novo design of discrete, stable 3(10)-helix peptide assemblies, Nature 607 (7918) (2022) 387–392.
[79] M. Martinez-Goikoetxea, A.N. Lupas, New protein families with hendecad coiled coils in the proteome of life, J. Struct. Biol. 215 (3) (2023) 108007.
[80] S.M. Khan, et al., Differential scanning calorimetry of bovine rhodopsin in rod-outer-segment disk membranes, Eur. J. Biochem. 200 (1) (1991) 53–59.
[81] J.S. Landin, M. Katragadda, A.D. Albert, Thermal destabilization of rhodopsin and opsin by proteolytic cleavage in bovine rod outer segment disk membranes, Biochemistry 40 (37) (2001) 11176–11183.
[82] S.C. Kwok, R.S. Hodges, *Clustering of large Hydrophobes in the hydrophobic Core of two-stranded α-helical coiled-coils controls protein folding and stability*, J. Biol. Chem. 278 (37) (2003) 35248–35254.
[83] M. Munson, et al., Redesigning the hydrophobic core of a four-helix-bundle protein, Protein Sci. 3 (11) (1994) 2015–2022.
[84] D. Schneider, et al., Thermostability of membrane protein helix–helix interaction elucidated by statistical analysis, FEBS Lett. 532 (1) (2002) 231–236.
[85] D.C. Mitchell, B.J. Litman, Effect of cholesterol on molecular order and dynamics in highly polyunsaturated phospholipid bilayers, Biophys. J. 75 (2) (1998) 896–908.
[86] A. Polozova, B.J. Litman, Cholesterol dependent recruitment of di22:6-PC by a G protein-coupled receptor into lateral domains, Biophys. J. 79 (5) (2000) 2632–2643.
[87] Q. Chen, et al., The rhodopsin-arrestin-1 interaction in bicelles, Methods Mol. Biol. 1271 (2015) 77–95.
[88] T. Zhuang, et al., Involvement of distinct arrestin-1 elements in binding to different functional forms of rhodopsin, Proc. Natl. Acad. Sci. USA 110 (3) (2013) 942–947.
[89] M. Heck, K.P. Hofmann, G-protein-effector coupling: a real-time light-scattering assay for transducin-phosphodiesterase interaction, Biochemistry 32 (32) (1993) 8220–8227.
[90] A. Alshalfouh, et al., Electrochemistry of CdSe quantum dots studied by single molecule spectroscopy, ChemElectroChem 6 (6) (2019) 1884–1893.
[91] K.W. Koch, et al., Functional coupling of a Ca2+/calmodulin-dependent nitric oxide synthase and a soluble guanylyl cyclase in vertebrate photoreceptor cells, EMBO J. 13 (14) (1994) 3312–3320–3320.
[92] M.M. Bradford, A rapid and sensitive method for the quantitation of microgram quantities of protein utilizing the principle of protein-dye binding, Anal. Biochem. 72 (1) (1976) 248–254.
[93] K.E. Van Holde, W.C. Johnson, P.S. Ho, Principles of Physical Biochemistry, Pearson/Prentice Hall, 2006.
[94] N.J. Greenfield, Using circular dichroism collected as a function of temperature to determine the thermodynamics of protein unfolding and binding interactions, Nat. Protoc. 1 (6) (2006) 2527–2535.